Catalyst Poisoning by Amorphous Carbon during Carbon Nanotube Growth: Fact or Fiction?

Christoph Schünemann,[†,‡,*] Franziska Schäffel,[§] Alicja Bachmatiuk,[†] Ute Queitsch,[†] Maria Sparing,[†] Bernd Rellinghaus,[†] Khalid Lafdi,[⊥] Ludwig Schultz,[†] Bernd Büchner,[†] and Mark H. Rümmeli[†,‡,*]

[†]IFW Dresden, P.O. Box 270116, D-01171 Dresden, Germany, [‡]Technische Universität Dresden, D-01062 Dresden, Germany, [§]Department of Materials, University of Oxford, Parks Road, Oxford OX1 3PH, United Kingdom, and [⊥]University of Dayton, Dayton, Ohio 45469, United States

ABSTRACT

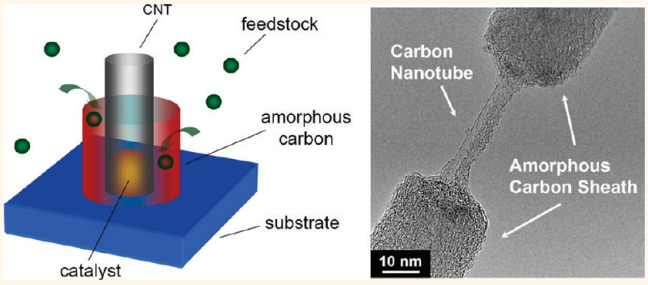

The influence of amorphous carbon on FePt catalyst particles under chemical vapor deposition conditions typically applied for CNT growth is examined through two routes. In the first, FePt catalyst particles supported on alumina are exposed to a well-established cyclohexane thermal CVD reaction at various temperatures. At higher temperatures where self-pyrolysis leads to copious amorphous carbon and carbon tar formation, carbon nanotubes are still able to form. In the second route, an amorphous carbon film is first deposited over the catalyst particles prior to the CVD reaction. Even for reactions where further amorphous carbon is deposited due to self-pyrolysis, graphitization is still demonstrated. Our findings reveal that the presence of amorphous carbon does not prevent catalytic hydrocarbon decomposition and graphitization processes. We also show an additional catalytic reaction to be present, catalytic hydrogenation, a process in which carbon in contact with the catalyst surface reacts with H_2 to form CH_4.

KEYWORDS: catalysis · carbon · growth factors · nanotubes · synthesis design

Carbon nanotubes (CNTs) exhibit unique electrical and mechanical properties which make them promising candidates for integration into nanoscale electronic devices[1] or compound materials.[2] A wide variety of methods have been developed to fabricate CNTs, including arc discharge,[3] laser ablation,[4,5] and chemical vapor deposition (CVD).[6] Among these, CVD is the most technically important since it can be achieved at low temperature and is upscalable.[6,7] Nevertheless, the finer details of CNT growth mechanisms remain poorly understood. The vapor–liquid–solid (VLS) model first put forward by Baker *et al.*[8] or variations of this model are usually implemented to describe CNT growth. In the VLS model, carbon atoms derived from the decomposition of a gaseous hydrocarbon feedstock at the catalyst particle surface first dissolve into the particle, forming a liquid carbide phase which then precipitates in the form of a CNT or other sp^2 carbon products. The vapor–solid model[9] is an extension of the VLS model and is able to explain the formation of CNT at low growth temperatures where it is assumed that the catalyst does not reach a liquid phase. In this model, the dissociated carbon migrates only over the catalyst surface in contrast to the VLS model which assumes bulk diffusion. In both growth models, encapsulation of the catalyst with amorphous carbon is argued to inactivate CNT growth and is often referred to as *catalyst poisoning*. The inactivation or poisoning process of catalyst particles by amorphous carbon is rarely discussed in the literature. Indeed, although termination of CNT growth is often attributed to amorphous carbon poisoning, as pointed out by Reilly and Whitten,[10] how this actually happens has yet to be demonstrated. Indirect studies in which the presence of water vapor, oxygen, or hydrogen radicals is present often lead to improved growth.[11,12] The improved growth is usually attributed to these additives reducing amorphous species at the catalyst surface which results in an enhanced catalyst activation.[13] However, these statements stand in stark contrast to various more direct experimental observations, suggesting a rather different scenario. In a study by Derbyshire *et al.*[14] as far back in 1975, they showed graphite formation by depositing amorphous carbon on iron, cobalt, and nickel foils. They observed the carbon to diffuse out of the carbon-saturated films and then rearrange

* Address correspondence to christoph.schuenemann@iapp.de, m.ruemmeli@ifw-dresden.de.

Received for review August 13, 2011 and accepted October 24, 2011.

Published online October 24, 2011
10.1021/nn2031066

itself on the surface as graphite upon appropriate annealing. These days, the technique is popular for the formation of graphene.[15−18] In addition, an interesting *in situ* study showed molten Ni, Co, and Fe particles moving on the surface of amorphous carbon, leaving crystalline graphitic tracks behind.[19,20] All of these studies show that metal catalysts directly in contact with amorphous carbon can crystallize the carbon to its most thermodynamically stable form, graphite. They suggest that amorphous carbon does not poison catalyst particles.

In order to fill the unstudied gap of amorphous carbon−metallic catalyst particle interactions under chemical vapor deposition (CVD) conditions typically applied for CNT growth, we exploited two avenues. In the first, we systematically investigated the behavior of FePt catalyst particles (two diameter sets) supported on alumina after exposure to a well-established cyclohexane thermal CVD reaction[21] for various temperatures, including at higher temperatures where self-pyrolysis leads to significant amorphous carbon formation and higher hydrocarbons.[22] In the second route, the catalyst particles were coated by amorphous carbon through the intentional deposition of an amorphous film prior to the CVD reaction. For comparison, the latter were also annealed under high vacuum conditions to differentiate the role of heat and feedstock gases. The studies show that the presence of amorphous carbon does not prevent catalytic hydrocarbon decomposition and graphitization processes. In fact, they reveal an additional catalytic reaction to be present, catalytic hydrogenation, a process in which carbon in contact with the catalyst surface reacts with H_2 to form CH_4.

RESULTS

Systematic studies were carried out to explore the growth of CNT *via* FePt CVD across a broad range of temperatures (590−890 °C). Two sets of catalyst particles were used, one with a mean diameter of 3.6 nm (standard deviation = 0.9 nm) and the second with a smaller particle distribution having a mean diameter of 1.6 nm (standard deviation = 0.4 nm). The use of two sets of catalysts allows us to evaluate catalyst size dependencies and provides additional reproducibility assessment. Figure 1a,b shows TEM images typifying the particles produced *via* the employed inert gas condensation route. Panels c and d show how the substrates appear when examined with SEM after the CVD reaction (785 °C).

Typically, the substrates have randomly oriented and curled CNT on their surface. To better investigate the structure of the CNT, TEM studies were conducted for both diameter distributions for each temperature explored. Representative examples are provided in Figure 2. With respect to the lower temperature region

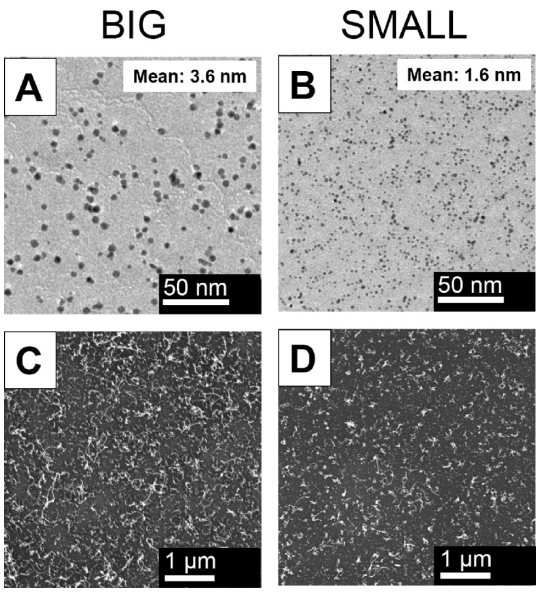

Figure 1. TEM micrographs showing the pristine FePt catalyst particles on a carbon membrane: (A) large diameter (mean = 3.6 nm), (B) small diameter (mean = 1.6 nm). SEM micrographs typifying synthesized carbon nanotubes on the substrate. CNT grown from large particles (C) and small particles (D) (reaction temperature = 785 °C).

between 550 and 670 °C, no nanotubes were observed when using the "small" initial catalyst particles. Only large metallic particles encapsulated with numerous graphitic layers were observed (*e.g.*, Figure 2F). In this same temperature region (between 550 and 670 °C), carbon nanotubes are obtained with the larger particles. A thorough statistical analysis of over 200 tubes (from TEM micrographs) for each reaction temperature shows that between 550 and 670 °C the tubes are primarily double-walled carbon nanotubes (DWNTs). Figure S1 in the Supporting Information shows a typical Raman spectrum and statistical analysis (derived from TEM analysis) on the high yield DWNT. The DWNT mean diameters are stable in this region (*ca.* 4.0 nm) and closely match that of the starting particles (3.6 nm), suggesting the catalyst particles template the DWNT outer diameters, in agreement with previous findings.[23−25] The stability of the tube outer diameters in this temperature region is shown in Figure 3, region 1. The TEM studies also revealed very few catalyst particles residing at the ends of the tubes, and this implies that they grow *via* the base growth mode as was previously found for gas-phase prepared iron catalyst particles.[23]

Above 680 °C and below 800 °C, changes can be observed for all samples using both the large and small FePt catalyst sets. With regard to the small particle set, SEM and TEM observations show the presence of carbon nanotubes with outer diameters between 4 and 6 nm (as determined from TEM analysis). The CNT diameters slightly increase at higher temperatures, and between 750 and 800 °C, small amounts of amorphous

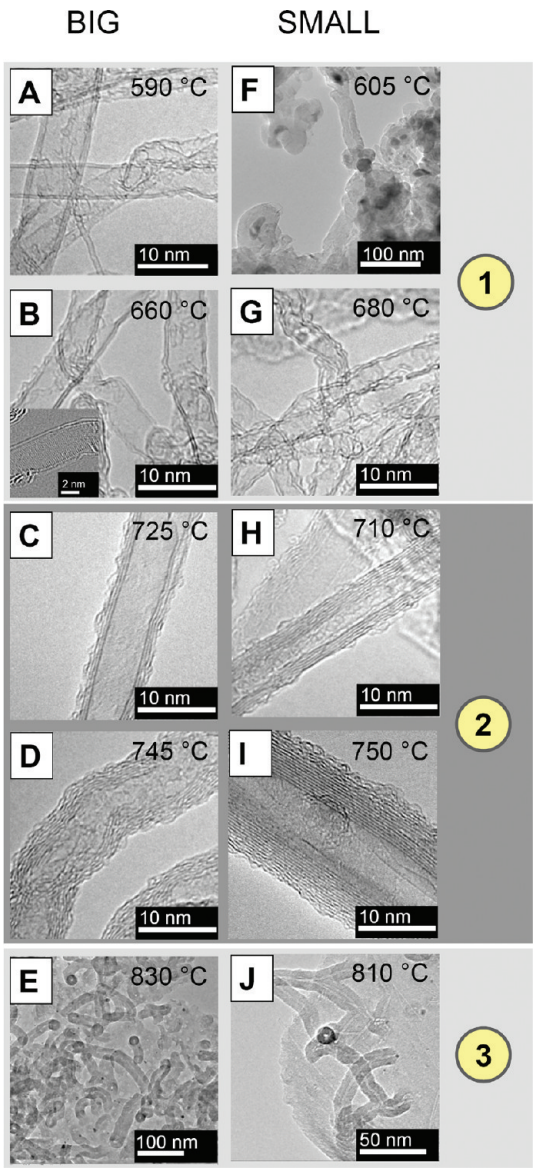

Figure 2. TEM micrographs showing various carbon nanotubes synthesized at different temperatures using large catalyst particles (left column) and small catalyst particles (right column). The number labeling to the right corresponds to the numbered regions highlighted in Figure 3.

carbon can be observed on the surface of the tubes. In addition, traces of an oily substance, herein referred to as carbon tar, can be seen to condense outside the hot zone of the reactor. The CNTs obtained from the smaller catalyst particle set suggest a more delayed increase in their outer diameter and number of walls as compared to the smaller catalyst size. The increasing diameters and their correlation with catalyst size and number of walls is discussed in greater depth further on. The mean CNT diameter enlargement with temperature (between 680 and 800 °C) is shown in region 2 of Figure 3.

Regardless of the starting catalyst set, above 800 °C, all samples show a steep increase in mean diameter as can be observed in region 3 of Figure 3. Closer examination of

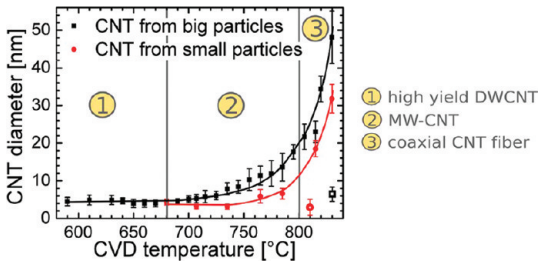

Figure 3. Mean carbon nanotube outer diameter *vs* reaction temperature for both large particles (black) and small catalyst particles (red). Curves are a guide to the eye. The hollow square point in black and hollow circular point in red show the mean CNT diameters *after* annealing in air to burn off the amorphous carbon coating. Region 1: stable CNT mean diameter. Region 2: increasing CNT mean diameter. Region 3: CNTs are increasingly coated with amorphous carbon.

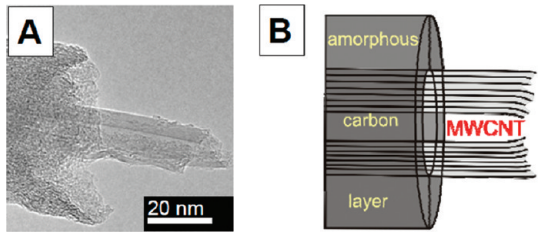

Figure 4. TEM image and schematic showing the core–shell structure of tubes formed at higher temperatures (830 °C). The core consists of a carbon nanotube. The shell is formed of amorphous carbon.

these structures through TEM investigations shows that they consist of narrow few-walled CNTs with a thick amorphous carbon coating. The existence of the amorphous carbon is due to the self-pyrolysis of cyclohexane at these temperatures. Typically, the self-pyrolysis of hydrocarbons leads to amorphous carbon and carbon tar byproduct which consist predominantly of polycyclic aromatic hydrocarbons (PAHs). In this study, around 800 °C and above, clear oily carbon tar and amorphous carbon deposits are present on the inner surface of the reaction tube. Even so, CNTs are still present, albeit coated with amorphous carbon. Greater details and a schematic of these all-carbon coaxial nanofibers are shown in Figure 4 and Figure S2 in the Supporting Information. The thickness of the outer amorphous carbon layer increases with increasing temperature. To investigate the diameters of the crystalline carbon nanotubes in the core, we annealed samples from each starting catalyst set in air at 200 °C for 30 min to gently remove the amorphous carbon coating. At the low burning temperature of 200 °C, only the amorphous carbon is removed since carbon nanotubes usually start to burn above 350 °C. Amorphous carbon begins to burn just before 200 °C.

Detailed TEM studies of these samples showed that the mean diameters of the core tubes (after burning off the amorphous coating) are smaller than that found for tubes fabricated at lower temperatures, that is, before the onset of the amorphous carbon shell formation

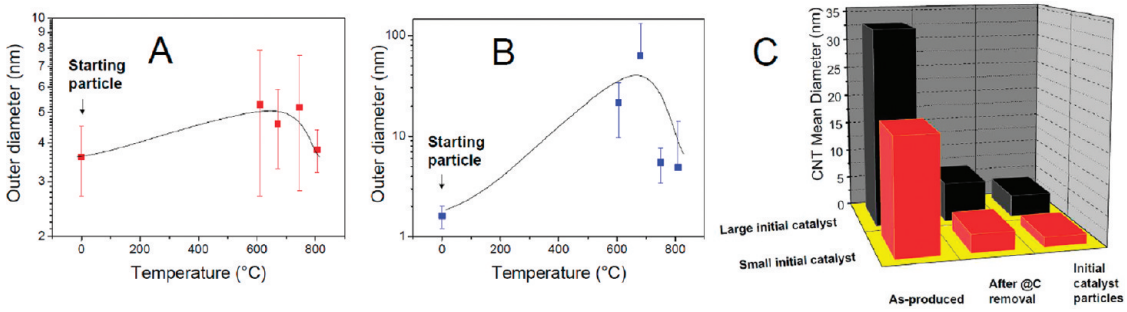

Figure 5. (A,B) Mean CNT outer diameters (after amorphous carbon removal) for various reaction temperatures relative to the starting catalyst particle size. (A) Large starting catalyst. (B) Small starting catalyst. n.b. Curves are a guide to the eye. (C) Statistical data showing the actual CNT mean diameter of CNTs produced at higher temperatures (600–800 °C) after selective removal of amorphous carbon (annealing at 200 °C in air). The initial catalyst particle mean diameter is provided for reference. Black, CVD temperature 830 °C; red, CVD temperature 810 °C.

(see bottom right corner of Figure 3, hollow points). Figure 5A,B shows the general trend in greater detail where the tube diameter (after selectively removing the amorphous coating) increases relative to the starting particle size for temperatures between 600 and near 800 °C, for both the larger and smaller particle diameters, respectively. Above this temperature, the real carbon nanotube diameter (*i.e.*, *without* the amorphous shell) is actually reduced. This trend is observed for both starting catalyst sample sets. In other words, the large outer diameter of the as-produced structures is primarily due to a thick amorphous coating. This can be seen in Figure 5C, which highlights the relative change between the mean as-produced core–shell diameters, the mean core tube diameters (amorphous carbon removed), and the mean starting particle diameters.

We also investigated the size of the catalyst particles after the CVD reaction, relative to the starting particle size. The post-synthesis particles' mean diameters are shown to increase and then decrease at temperatures around 800 °C. In addition, their distribution widths also increase and then decrease at the higher temperatures. These data are provided in the Supporting Information in Figure S3. This again indicates a correlation between the catalyst particle size and the resultant CNT outer diameter. This is further supported by the increasing number of walls forming the tube as its diameter increases, as shown in Figure 2 and Figure S4. This correlation remains even at higher temperatures where amorphous carbon deposits itself on the tubes. Figure S5 shows that core tubes (as obtained from the core–shell structures after amorphous carbon removal) that were formed from smaller catalyst particles have fewer walls than those formed from larger particles.

These characteristics are well explained with the catalyst volume to surface area model.[23,24,26] The model describes how the outer diameters of CNTs are templated by the catalyst particle diameter, and that the larger the particle, the greater the number of

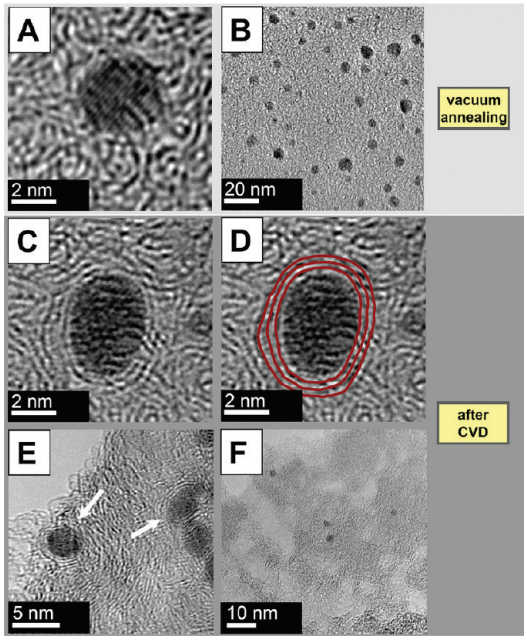

Figure 6. (A,B) TEM micrographs showing FePt nanoparticles embedded in an amorphous carbon film after annealing in vacuum (810 °C, 10 min). (C–E) TEM micrographs showing FePt nanoparticles encapsulated in graphitic shells after exposure to CVD reaction (cyclohexane, 810 °C, 10 min). (F) Micrograph showing etched amorphous carbon regions.

walls due to the increased carbon availability (volume-dependent) relative to the surface area, which in essence allows more hemispherical nucleation caps to form. It then becomes clear that the gradual increase in CNT mean diameter for temperatures below 800 °C can be explained by the catalyst particles increasing in size, *viz.*, the particles coalesce on the substrate and that the coalescence rate increases with temperature (see Figure S3). However, between 750 and 800 °C, cyclohexane starts to undergo self-pyrolysis, producing amorphous carbon species.[27] In the present study, the amorphous carbon deposits on the surface of the growing carbon nanotubes forming a linear core–shell structure in which the core is a crystalline carbon nanotube. Moreover, the diameter of the inner or core

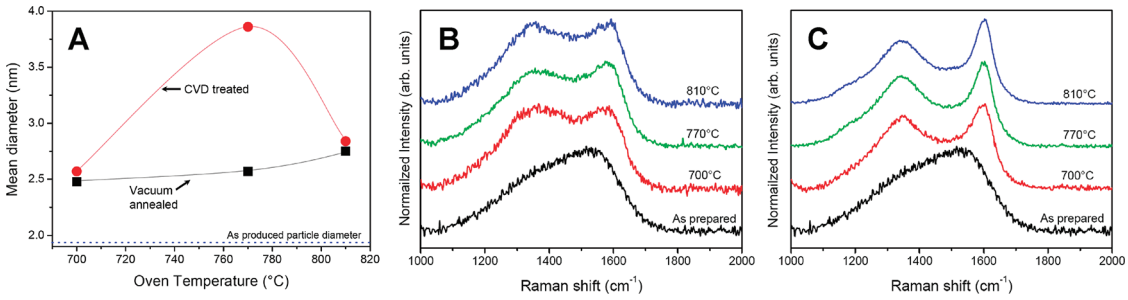

Figure 7. (A) Mean diameters of FePt nanoparticles coated with amorphous carbon after annealing in vacuum (square) and after exposure to CVD reaction (circle). Curves are a guide to the eye. (B,C) Raman spectra of annealed (B) and CVD-reacted samples (C) as compared to the as-prepared samples. The graphitization from the CVD-treated samples (C) is easily observed through the better defined G mode (*ca.* 1600 cm^{-1}) and D mode (1350 cm^{-1}).

CNT is small as compared to average CNT diameter before the onset of self-pyrolysis (see Figures 3 and 5). Our data also show reduced catalyst particle sizes at higher temperatures where self-pyrolysis is active. These data might suggest that amorphous carbon deposition on the substrate surface reduces the efficiency of particle coalescence. To test this hypothesis, we prepared various samples in which a 10 nm amorphous carbon layer was intentionally deposited over the deposited FePt nanoparticles. These samples were then annealed in vacuum and also exposed to CVD reactions at 700, 770, and 810 °C and subsequently subjected to TEM and Raman spectroscopy investigations. The TEM data from the vacuum-annealed samples (Figure 6A,B) showed FePt nanoparticles embedded in amorphous carbon, similar to the starting sample (data not shown). In the case of the CVD-treated samples, the nanoparticles were often observed to be surrounded by concentric graphitic rings; moreover, the amorphous carbon film contained etched regions (Figure 6C−F). The degree of graphitic layer formation around the catalyst particles and the number and size of the etched regions increases with temperature. Analysis of the catalyst particles showed no carbide phases. Only FePt phases were detected. The lack of carbide phases indicates either surface carbon diffusion occurs during graphitization or bulk carbon diffusion (precipitation) leading to graphitization. The general trend of increasing numbers of graphitic layers with increasing particle size points to bulk diffusion; that is, as the catalyst to volume surface area increases, more carbon is available to form graphitic shells.

Figure 7A presents a statistical analysis of the particle mean diameters for all samples intentionally coated with amorphous carbon. For those annealed in vacuum, a slight but steady increase in the particles' mean diameter was observed. However, the amorphous carbon-coated nanoparticles exposed to the CVD reactions showed a significant increase in mean diameter (and diameter distribution) when raising the temperature from 700 to 770 °C, which then dropped when further raising the temperature to 810 °C. This behavior correlates very well with observations from the conventional CVD studies discussed above (see Figure 5A,B). However, the maximum particle mean diameter (with intentional amorphous carbon coating) occurs at a higher temperature (∼770 °C) as compared to that obtained for the standard CVD case (∼680 °C) where little or no amorphous carbon forms. This suggests that the presence of amorphous carbon reduces catalyst mobility on the substrate. However, the carbon feed rate can account for this effect more accurately. The parabolic trend of the mean nanoparticle size with increasing CVD reaction temperature can be explained as follows: Initially, as the temperature increases, the added energy increases catalyst particle mobility. Increased temperatures also lead to greater carbon feed rates which could enable the catalyst particles to reach a carbide phase more rapidly. This can accelerate liquefaction and coalesce.[28] Moreover, a carbide particle/substrate may be weaker than for the noncarbide phase, leading to increased particle mobility. However, the increase in carbon supply rate also means that the time required to reach nucleation will be reduced, *viz.* the nucleation rate increases. Hence a competing process to particle coalescence is the nucleation rate. Once the nucleation rate is sufficiently high, nucleation can occur before the catalyst particles have sufficient time to coalesce. In the case of an amorphous carbon film residing over the catalyst particles, the carbon feed rate will be reduced since the feedstock and cracked components from the feedstock must first diffuse through the amorphous carbon to reach the catalyst particle. Hence the mean particle diameter maximum should occur at a higher reaction temperature, exactly as we observe experimentally. Further experimental evidence in this vein can be found in Figure 3, where the diameter increase in region 2 occurs at higher temperatures for the smaller particles as compared to the larger ones. This can be explained by a larger *relative* amorphous carbon layer existing for the smaller particles. Raman spectroscopic data were also collected for the amorphous coated samples before and after their annealing and CVD reactions. The results matched the TEM observations

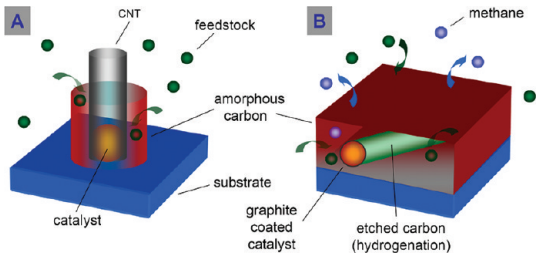

Figure 8. (A) Schematic illustrating CNT growth despite the presence of a self-pyrolyzing hydrocarbon feedstock and heavy amorphous carbon deposition. (B) Schematic showing graphitic shell formation around catalyst particles and etching of amorphous carbon by hydrogenation for FePt nanoparticles with a 10 nm deposited amorphous carbon layer and subsequent exposure to a CVD reaction.

very well, namely, no graphitization is observed when only annealing the samples coated with amorphous carbon (Figure 7B). Exposing them to CVD reactions leads to graphitization as shown by the clear formation of well-defined G and D modes at *ca.* 1600 and 1350 cm^{-1}, respectively, despite the dominant amorphous carbon background. The existence of the defined G and D modes indicate sp^2 carbon formation[29] (Figure 7C), in agreement with the TEM observations.

DISCUSSION AND CONCLUSION

The data are revealing in that in all of the CVD experiments the catalyst particles are able to graphitize carbon despite the presence of amorphous carbon deposits. In the case where no amorphous carbon film is intentionally deposited on the catalyst particles, CNT are obtained, even at high temperatures where the feedstock undergoes self-pyrolysis leading to large amorphous carbon and carbon tar deposition. However, with an intentional amorphous carbon coating over the catalyst particles prior to the CVD reaction, only graphitic encapsulation of the particles is obtained. This can be attributed to the amorphous carbon film preventing lift-off of the nucleation caps and hence forcing encapsulation. In the conventional CVD case, the rapid nucleation rate at higher temperatures (discussed above) means that nucleation of a CNT *via* hemispherical cap lift-off can occur before the amorphous carbon deposits are able to block this process. Moreover, simply annealing the supported FePt nanoparticles covered in an amorphous layer does not lead to any significant graphitization and no etching of the amorphous carbon film is observed, contrary to that found when exposing the samples to a CVD reaction. This shows that the feedstock and/or cracked components from the feedstock are able to permeate amorphous carbon and reach the catalyst particles, enabling them to catalytically form sp^2 carbon, albeit at a reduced rate. The etching of the amorphous carbon itself can be explained by a catalytic hydrogenation process in which H_2 reacts with carbon at the catalyst surface forming CH_4 (see reaction 1).

$$C_{(s)} + 2H_{2(g)} \rightarrow CH_{4(g)} \quad (1)$$

The process is well-known as a technique to etch crystallographically oriented tracks in graphene.[30−32] In our studies, no tracks are observed; only etched patches are present, which is due to the lack of structural order (amorphous carbon). Simple thermodynamic calculations to determine the relative amounts and type of byproduct when thermally cracking cyclohexane (see Figure S6) show that significant levels of H_2 are present in the reaction, further supporting the catalytic hydrogenation process. The thermodynamic calculations also show that the level of hydrogen radicals is minute and is therefore not likely to play a major role in etching carbon species. Hence, the precipitation of carbon from catalyst particles forming CNTs (and graphitic encapsulation) occurs in competition with the catalytic hydrogenation process. Both of these catalytic processes, namely, CNT growth continuing even in the presence of a self-pyrolyzing hydrocarbon feedstock (Figure 8A) as well as graphitic shell formation around catalyst particles and etching of amorphous carbon by hydrogenation (Figure 8B), highlight that the catalyst particles are not poisoned by amorphous carbon and carbon tar. The argument that amorphous carbon halts nanotube growth by poisoning the catalyst needs re-examination.

EXPERIMENTAL METHODS

The FePt (1:1) catalyst nanoparticles were synthesized in a single step *via* inert gas condensation.[23] Quantitative analysis of EDX spectra obtained from particle ensembles confirmed an elemental content of 50 ± 2 atom % Fe or Pt. For CNT production, the particles are deposited onto a thermally oxidized silicon substrate with an additional 10 nm Al_2O_3 layer. The CVD reaction took place in a horizontal tube furnace (quartz tube inner diameter 9 mm, length 70 cm). Prior to synthesis, the oven tube was evacuated to $>2 \times 10^{-5}$ mbar. Once the oven reached the desired synthesis temperature, it was shifted over the CVD substrate. The synthesis temperature was varied from 560 to 830 °C. First, a reduction step by purging hydrogen at 0.1 slpm (standard liters per minute) at a constant pressure of 60 mbar through the reactor for 10 min was carried out. Thereafter, the hydrogen was pumped out and the carbon feedstock, cyclohexane (C_6H_{12}), was gently introduced into the reactor and kept at a constant pressure of 50 mbar for 5 min.[27] Finally, the C_6H_{12} was pumped out and the furnace swiftly shifted away from the substrate to allow rapid cooling.

Samples which were annealed were treated with a similar protocol as discussed above, except no hydrocarbon was introduced and a vacuum $>10^{-6}$ mbar was implemented.

The as-prepared FePt nanoparticles, the CVD-prepared samples, and the annealed samples were characterized by transmission electron microscopy (TEM) with a FEI Tecnai G2 20 microscope operating at 200 kV, a C_S-corrected FEI Titan^3 80-300 operating at 80 kV, and a C_S-corrected JEOL 2010F operating at 80 kV. TEM samples were prepared by mechanically pressing standard TEM

(Cu and lacey carbon on Cu) grids on CVD-prepared and annealed samples. The as-prepared FePt particles were prepared on carbon film TEM grids placed in the particle reactor during their actual deposition. Scanning electron microscopy (SEM) was conducted using a LEO Gemini 1530 at 5 kV. Raman spectroscopy was carried out on a Bruker IFS100 spectrometer (1064 nm) and Thermo Fischer SmartRaman DXR (532 nm).

Acknowledgment. F.S. and A.B. thank the Alexander von Humboldt Stiftung and the BMBF, M.S. the Studienstiftung des deutschen Volkes, and M.H.R. the EU (ECEMP) and the Freistaat Sachsen and the DFG (RU 1540/8-1). We gratefully acknowledge help from D. Makarov and R. Kaltofen for help with thin film preparations.

Supporting Information Available: Raman spectrum of DWNT. Statistical analysis of catalyst particles before and after CVD reactions. Statistical analysis of CNT number of walls. Thermodynamic calculation data for thermal cracking of cyclohexane. This material is available free of charge *via* the Internet at http://pubs.acs.org.

REFERENCES AND NOTES

1. Tans, S. J.; Verschueren, A. R. M.; Dekker, C. Room-Temperature Transistor Based on a Single Carbon Nanotube. *Nature* **1998**, *393*, 49–52.
2. Kuzumaki, T.; Miyazawa, K.; Ichinose, H.; Ito, K. Processing of Carbon Nanotube Reinforced Aluminum Composite. *J. Mater. Res.* **1998**, *13*, 2445–2449.
3. Iijima, S. Helical Microtubules of Graphitic Carbon. *Nature* **1991**, *354*, 56–58.
4. Guo, T.; Nikolaev, P.; Thess, A.; Colbert, D. T.; Smalley, R. E. Catalytic Growth of Single-Walled Nanotubes by Laser Vaporization. *Chem. Phys. Lett.* **1995**, *243*, 49–54.
5. Rümmeli, M. H.; Borowiak-Palen, E.; Gemming, T.; Pichler, T.; Knupfer, M.; Kalbác, M.; Dunsch, L.; Jost, O.; Silva, S. R. P.; Pompe, W.; *et al.* Novel Catalysts, Room Temperature and the Importance of Oxygen for the Synthesis of Single Wall Carbon Nanotubes. *Nano Lett.* **2005**, *5*, 1209–1215.
6. Li, W. Z.; Xie, S. S.; Qian, L. X.; Chang, B. H.; Zou, B. S.; Zhou, W. Y.; Zhao, R. A.; Wang, G. Large-Scale Synthesis of Aligned Carbon Nanotubes. *Science* **1996**, *274*, 1701–1703.
7. Lee, C. J.; Park, J.; Kim, J. M.; Huh, Y.; Lee, J. Y.; No, K. S. Low-Temperature Growth of Carbon Nanotubes by Thermal Chemical Vapor Deposition Using Pd, Cr, and Pt as Co-Catalyst. *Chem. Phys. Lett.* **2000**, *327*, 277–283.
8. Baker, R. T. K.; Barber, M. A.; Harris, P. S.; Feates, F. S.; Waite, R. J. Nucleation and Growth of Carbon Deposits from the Nickel Catalyzed Decomposition of Acetylene. *J. Catal.* **1972**, *26*, 51–62.
9. Hofmann, S.; Csanyi, G.; Ferrari, A. C.; Payne, M. C.; Robertson, J. Surface Diffusion: The Low Activation Energy Path for Nanotube Growth. *Phys. Rev. Lett.* **2005**, *95*, 036101/1–4.
10. Reilly, P. T. A.; Whitten, W. B. The Role of Free Radical Condensates in the Production of Carbon Nanotubes During the Hydrocarbon CVD Process. *Carbon* **2006**, *44*, 1653–1660.
11. Hata, K.; Futaba, D. N.; Mizuno, K.; Namai, T.; Yumura, M.; Iijima, S. Water-Assisted Highly Efficient Synthesis of Impurity-Free Single-Walled Carbon Nanotubes. *Science* **2004**, *306*, 1362–1364.
12. Zhang, G.; Mann, D.; Zhang, L.; Javey, A.; Li, Y.; Yenilmez, E.; Wang, Q.; McVittie, J. P.; Nishi, Y.; Gibbons, J.; *et al.* Ultra-High-Yield Growth of Vertical Single-Walled Carbon Nanotubes: Hidden Roles of Hydrogen and Oxygen. *Proc. Natl. Acad. Sci. U.S.A.* **2005**, *102*, 16141–16145.
13. Yoshihara, N.; Ago, H.; Tsuji, M. Chemistry of Water-Assisted Carbon Nanotube Growth over Fe−Mo/MgO Catalyst. *J. Phys. Chem. C* **2007**, *111*, 11577–11582.
14. Derbyshire, F. J.; Presland, A. E. B.; Trimma, D. L. Graphite Formation by the Dissolution−Precipitation of Carbon in Cobalt, Nickel and Iron. *Carbon* **1975**, *13*, 111–113.
15. Zheng, M.; Takei, K.; Hsia, B.; Fang, H.; Zhang, X.; Ferralis, N.; Ko, H.; Chueh, Y.-L.; Zhang, Y.; Maboudian, R.; *et al.* Metal-Catalyzed Crystallization of Amorphous Carbon to Graphene. *Appl. Phys. Lett.* **2010**, *96*, 063110/1–3.
16. Liu, N.; Fu, L.; Dai, B.; Yan, K.; Liu, X.; Zhao, R.; Zhang, Y.; Liu, Z. Universal Segregation Growth Approach to Wafer-Size Graphene from Non-Noble Metals. *Nano Lett.* **2011**, *11*, 297–303.
17. Orofeo, C. M.; Ago, H.; Hu, B.; Tsuji, M. Synthesis of Large-Area, Homogeneous, Single Layer Graphene by Annealing Amorphous Carbon on Co and Ni. *Nano Res.* **2011**, *4*, 531–540.
18. Berndt, M.; Abrasonis, G.; Kovacs, Gy. J.; Krause, M.; Munnik, F.; Heller, R.; Kolitsch, A.; Möller, W. Bulk Diffusion Induced Structural Modifications of Carbon-Transition Metal Nanocomposite Films. *J. Appl. Phys.* **2011**, *109*, 063503/1–11.
19. Grodetskii, A. E.; Evko, E. I.; Zakharov, A. P. Crystallisation of Amorphous Carbon by Moving Nickel Particles. *Fizika Tverdogo Tela* **1976**, *18*, 619–621.
20. Krivoruchko, O. P.; Zaikovskii, V. I. A New Phenomenon Involving the Formation of Liquid Mobile Metal-Carbon Particles in the Low-Temperature Catalytic Graphitization of Amorphous Carbon by Metallic Fe, Co and Ni. *Mendeleev Commun.* **1998**, *3*, 97–100.
21. Schäffel, F.; Kramberger, C.; Rümmeli, M. H.; Grimm, D.; Mohn, E.; Gemming, T.; Pichler, T.; Rellinghaus, B.; Büchner, B.; Schultz, L. Nanoengineered Catalyst Particles as a Key for Tailor-Made Carbon Nanotubes. *Chem. Mater.* **2007**, *19*, 5006–5009.
22. Franklin, N. R.; Li, Y.; Chen, R. J.; Javey, A.; Dai, H. Patterned Growth of Single-Walled Carbon Nanotubes on Full 4-Inch Wafers. *Appl. Phys. Lett.* **2001**, *79*, 4571/1–3.
23. Rümmeli, M. H.; Schäffel, F.; Kramberger, C.; Gemming, T.; Bachmatiuk, A.; Kalenczuk, R. J.; Rellinghaus, B.; Büchner, B.; Pichler, T. Oxide-Driven Carbon Nanotube Growth in Supported Catalyst CVD. *J. Am. Chem. Soc.* **2007**, *129*, 15772–15773.
24. Rümmeli, M. H.; Schäffel, F.; Bachmatiuk, A.; Adebimpe, D.; Trotter, G.; Börrnert, F.; Scott, A.; Coric, E.; Sparing, M.; Rellinghaus, B.; *et al.* Investigating the Outskirts of Catalyst Particles in Supported Catalytic CVD Carbon Nanotubes Growth. *ACS Nano* **2010**, *4*, 1146–1152.
25. Kingston, C. T.; Simard, B. Recent Advances in Laser Synthesis of Single-Walled Carbon Nanotubes, Recent Advances in Laser Synthesis of Single-Walled Carbon Nanotubes. *J. Nanosci. Nanotechnol.* **2006**, *6*, 1225–1232.
26. Rümmeli, M. H.; Kramberger, C.; Loeffler, M.; Jost, O.; Bystrzejewski, M.; Grueneis, A.; Gemming, T.; Pompe, W.; Büchner, B.; Pichler, T. Catalyst Volume to Surface Area Constraints for Nucleating Carbon Nanotubes. *J. Phys. Chem. B* **2007**, *111*, 8234–8241.
27. Ayala, P.; Grüneis, A.; Grimm, D.; Kramberger, C.; Engelhard, R.; Rümmeli, M. H.; Schumann, J.; Kaltofen, R.; Büchner, B.; Schaman, C.; *et al.* Cyclohexane Triggers Staged Growth of Pure and Vertically Aligned Single Wall Carbon Nanotubes. *Chem. Phys. Lett.* **2008**, *454*, 332–336.
28. Borowiak-Palen, E.; Bachmatiuk, A.; Rümmeli, M. H.; Gemming, T.; Kruszynska, M.; Kalenczuk, R. J. Modifying CVD Synthesized Carbon Nanotubes *via* the Carbon Feed Rate. *Physica E* **2008**, *40*, 2227–2230.
29. Costa, S.; Borowiak-Palen, E.; Kruszynska, M.; Bachmatiuk, A.; Kalenczuk, R. J. Characterization of Carbon Nanotubes by Raman Spectroscopy. *Mater. Sci. Poland* **2008**, *26*, 433–441.
30. Datta, S. S.; Strachan, D. R.; Khamis, S. M.; Johnson, A. T. C. Crystallographic Etching of Few-Layer Graphene. *Nano Lett.* **2008**, *8*, 1912–1915.
31. Schäffel, F.; Wilson, M.; Bachmatiuk, A.; Rümmeli, M. H.; Queitsch, U.; Rellinghaus, B.; Briggs, G. A. D.; Warner, J. H. Atomic Resolution Imaging of the Edges of Catalytically Etched Suspended Few-Layer Graphene. *ACS Nano* **2011**, *5*, 1975–1983.
32. Schäffel, F.; Warner, J. H.; Bachmatiuk, A.; Rellinghaus, B.; Büchner, B.; Schultz, L.; Rümmeli, M. H. Shedding Light on the Crystallographic Etching of Multi-Layer Graphene at the Atomic Scale. *Nano Res.* **2009**, *2*, 695–705.